Bremsstrahlung Cross-Section Measurements for 50-kev Electrons*†

J. W. Motz and R. C. Placious
National Bureau of Standards, Washington, D. C.
(Received September 23, 1957)

The dependence of the bremsstrahlung differential cross section on photon energy and angle for 50-kev electrons ($\beta_0 \approx 0.4$) incident on a 10-μg/cm^2 gold target and a 17-μg/cm^2 aluminum target has been determined from measurements made with a scintillation spectrometer at angles ranging from 10 to 140 degrees. The experimental results are compared with the Sommerfeld-Kirkpatrick-Wiedmann cross sections multiplied by the relativistic correction factor $(1-\beta_0 \cos\theta)^{-2}$. For high photon energies (45 kev), the experimental results show good agreement with the theory at the peak intensity angles, approximately 50 and 60 degrees for gold and aluminum, respectively, but at the extreme angles there are differences of about 50% with the theory. For low photon energies (10 kev), discrepancies with the theory also increase at the extreme angles, with maximum differences of about 30% for aluminum and 40% for gold. Good agreement is obtained between theory and experiment over the whole angular range for 45-kev photons emitted from the aluminum target, when rough estimates of retardation and screening effects are also included in the theory. The experimental values for the Heitler parameter, $\phi_{\text{rad}}/\bar{\phi}$, are 5.5±0.6 and 6.7±0.7 for aluminum and gold respectively, compared to the theoretical value (including the above relativistic correction factor) of approximately 6.9 for *both* aluminum and gold.

I. INTRODUCTION

THE Sommerfeld theory[1] is used as the starting point for *low*-energy bremsstrahlung calculations. Sommerfeld derived the bremsstrahlung differential cross-section formula for the single process in which a photon is emitted in a given direction with a fixed recoil angle for the electron. In Sommerfeld's calculations, nonrelativistic Coulomb wave functions are used, and screening and retardation effects are neglected. The Sommerfeld dipole matrix element has been evaluated by Kirkpatrick and Wiedmann,[2] and they have calculated the bremsstrahlung cross section integrated over the direction of the emerging electron for particular energies of the photon and of the initial electron. Other nonrelativistic calculations[3] that are available are more restrictive, or are not as convenient to use as the Kirkpatrick-Wiedmann results. As yet, no exact cross-section calculations have been made which completely account for screening and retardation effects[4] in the nonrelativistic region.

Very few experimental determinations of the bremsstrahlung cross section are available which provide a satisfactory test of the nonrelativistic Sommerfeld theory. In the nonrelativistic energy region there are difficult experimental problems: for example, very thin targets (about 0.1 μg/cm^2) are required which do not readily withstand the large electron currents needed to produce adequate photon intensities. Because of such difficulties, low-energy thin-target bremsstrahlung measurements have been confined to the energy region, $0.2 \leq \beta_0 \leq 0.5$, where for an initial electron velocity v_0, β_0 is equal to v_0/c. Since these values of β_0 are not negligible compared to unity, the Sommerfeld theory requires a relativistic correction before a comparison can be made with the experimental results.[5] Also the theory should be applied only for a limited energy region where it has been established that retardation and screening effects can be neglected.

In the early attempts[6] to measure the absolute bremsstrahlung cross section in the low-energy region, Ross filters were used to isolate one energy interval out of the continuous spectrum, and an air ionization chamber was used to determine the x-ray intensity. The results obtained by Smick and Kirkpatrick[6] and Clark and Kelly[6] for a given electron energy (15 and 32 kev, respectively), target (500 angstroms nickel and 360 angstroms aluminum, respectively), and photon emission angle (88 and 60 degrees, respectively), disagreed by a factor of at least two with the results derived from the Kirkpatrick-Wiedmann calculations. The only other cross-section measurements reported in this energy region were made by Amrehn,[7] who measured photon spectra with a proportional counter for a 90-degree photon emission angle and for 25- and 34-kev electrons incident on thin targets of carbon, aluminum, nickel, silver, and gold. Amrehn found that the ratio of the experimental to the Kirkpatrick-Wiedmann[2]

* A summary of this work was reported at the American Physical Society 1957 Summer Meeting [J. W. Motz and R. C. Placious, Bull. Am. Phys. Soc. Ser. II, 2, 310 (1957)].

† Work supported by the U. S. Atomic Energy Commission.

[1] A. Sommerfeld, *Wellenmechanik* (Frederick Ungar, New York, 1950), Chap. 7.

[2] P. Kirkpatrick and L. Wiedmann, Phys. Rev. **67**, 321 (1945).

[3] Nonrelativistic Born approximation calculations have been made by F. Sauter, Ann. Physik **18**, 486 (1933). The calculations of G. Elwert, Ann. Physik **34**, 178 (1939) are valid for $Ze^2\hbar^{-1}(v_2^{-1}-v_1^{-1}) \ll 1$. Other calculations of the differential cross-section formula for dipole radiation have been made by S. D. Drell and K. Huang, Phys. Rev. **99**, 686 (1955) and Thaler, Goldstein, McHale, and Biedenharn, Phys. Rev. **102**, 1567 (1956). Total bremsstrahlung cross-section calculations are given by J. M. Berger, Phys. Rev. **105**, 35 (1957) and K. Kummerer, Z. Physik **147**, 373 (1957).

[4] Calculations that include estimates of retardation effects have been made by M. Scheer and E. Zeitler, Z. Physik **140**, 642 (1955), but their results give only *relative* values for the cross section, and require a reliable evaluation of the bremsstrahlung polarization.

[5] Relativistic bremsstrahlung calculations break down in this range of values for β_0. See H. Bethe and W. Heitler, Proc. Roy. Soc. (London) **146**, 83 (1934); F. Sauter, Ann. Physik **20**, 404 (1934); H. Bethe and L. Maximon, Phys. Rev. **93**, 768 (1954).

[6] E. Smick and P. Kirkpatrick, Phys. Rev. **60**, 162 (1941); J. C. Clark and H. Kelly, Phys. Rev. **59**, 220 (1941).

[7] H. Amrehn, Z. Physik **144**, 529 (1956).

cross sections increases with atomic number from a value of approximately one for aluminum to 1.2 for gold. Other measurements in this energy region involving relative values of photon intensities have been made by Kulenkampff and others,[8] who find general agreement between the experimental results and the Sommerfeld predictions except for some differences in detail with regard to the spectral shape and angular distribution of the bremsstrahlung.

It is apparent from the few available results above that more measurements are needed in order to establish the degree of reliability of the Sommerfeld theory in the energy region where $\beta_0 \leq 0.5$. The present work was undertaken to determine the dependence of the bremsstrahlung differential cross section on photon energy, k, and emission angle, θ, for 50-kev electrons ($\beta_0 \approx 0.4$). Target materials with a low and high atomic number, Z, were used, and were thin enough so that the effects of electron multiple scattering could be neglected. The measurements were made with a scintillation spectrometer which measured photons with energies as low as approximately 7 kev. Although this type of spectrometer has a much poorer resolution than a proportional counter in the low-energy region, it has the advantage that its detection efficiency is higher by a few orders of magnitude and is more accurately known than that of the proportional counter. The cross sections are derived from measurements of the photon intensities at emission angles ranging from 10 to 140 degrees. From these data, we also obtain values for the cross section integrated over the photon emission angle and energy.

II. EXPERIMENTAL METHOD

A. Equipment and Procedure

The experimental arrangement for this work is shown in Fig. 1. The 50-kev electron beam is produced by a constant potential accelerator with a cascade-type generator. The beam diameter at the target position is approximately $\frac{1}{4}$ inch, and the target currents used for these measurements ranged from approximately 0.1 to 1 microampere. The bremsstrahlung emitted from the target at a given angle θ with respect to the incident electron direction, is detected by a scintillation spectrometer after passing through a 20-mil beryllium window in the target chamber and a 1-mil aluminum foil covering the NaI(Tl) crystal.

The scintillation spectrometer consists of a $\frac{1}{2}$-inch diameter, $\frac{1}{4}$-inch long NaI(Tl) crystal and a Du Mont 6292 photomultiplier tube. The crystal is mounted in a lead-lined copper container which has a $\frac{3}{16}$-inch diameter, $\frac{3}{32}$-inch thick entrance aperture. The spectrometer can detect photons with energies as low as 7 kev before the noise pulses of the photomultiplier tube become predominant. The pulse-height distribution is measured with a 12-channel differential pulse-height analyzer. The pulse-height response of this spectrometer to monoenergetic photons was measured with a source of Cd^{109} (22 kev: Ag K_α, 87 kev).[9] For the 22-kev photons, the energy resolution of the spectrometer that was found from the full width at half-maximum of the response curve is approximately 37%.

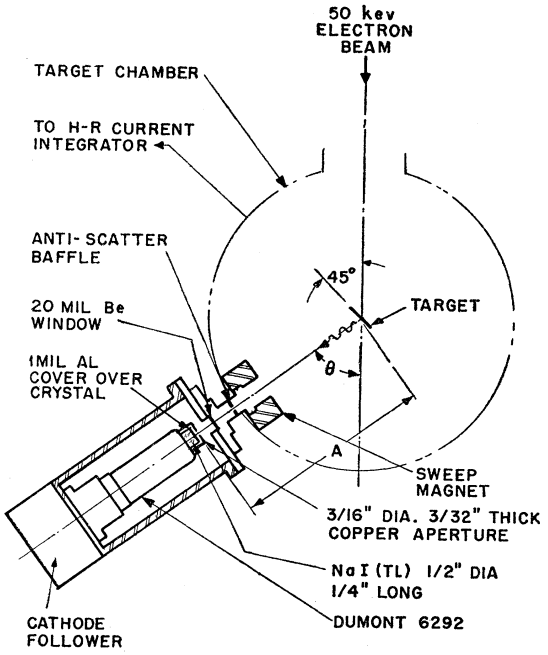

FIG. 1. Experimental arrangement for 50-kev bremsstrahlung measurements. The target materials were aluminum and gold with thicknesses of approximately 17 $\mu g/cm^2$ and 10 $\mu g/cm^2$, respectively. The values of θ were 10, 20, 30, 40, 50, 60, 70, 90, 110, and 140 degrees. The distance A is 11.5 inches for the angular region from 20 to 140 degrees and 12.6 inches for the θ value of 10 degrees.

Electrons incident on the target are collected by the target chamber which is electrically insulated from the grounded section of the accelerator. The target currents and the total charge collected in a given time interval are measured with a Higinbotham-Rankowitz current integrator[10] with approximately 2% accuracy.

The distance A in Fig. 1 between the target and the detector slit is 11.5 inches, except for the measurements made at 10 degrees where it was found desirable to use a distance of 12.6 inches and an aperture diameter of $\frac{5}{16}$ inch in order to minimize the effects of electron scattering in the chamber. With this geometry the detector slit has an angular resolution of about 1 degree.

Other relevant experimental details including a

[8] K. Bohm, Ann. Physik **33**, 315 (1938); R. Honerjager, Ann. Physik **38**, 33 (1940); H. Amrehn and H. Kulenkampff, Z. Physik **140**, 452 (1955); R. Kerscher and H. Kulenkampff, Z. Physik **140**, 632 (1955); H. Doffin and H. Kulenkampff, Z. Physik **148**, 496 (1957).

[9] *Nuclear Data*, National Bureau of Standards Circular No. 499 (U. S. Government Printing Office, Washington, D. C., 1950).

[10] W. A. Higinbotham and S. Rankowitz, Rev. Sci. Instr. **22**, 688 (1951).

description of the target chamber and the electronics are given elsewhere.[11]

The photon emission angles θ that were selected for the measurements were equal to 10, 20, 30, 40, 50, 60, 70, 90, 110, and 140 degrees. For each angle, measurements were made of the integrated charge incident on a given target and of the corresponding bremsstrahlung spectrum.

B. Targets

The target materials selected for these measurements were gold and aluminum. The important features of the targets that must be taken into account in the determination of the cross sections are their thickness, uniformity, and purity.

The criterion for the selection of a thin target is that the electron scattering and energy loss in the target is small enough to be neglected. As an estimate for the proper thickness to use for 50-kev electrons, we may expect that a target is thin enough if the obliquity of the electrons in passing through the foil is as small as 2%, that is if

$$1-\langle\cos\alpha\rangle_{Av}\approx\langle\alpha^2\rangle_{Av}/2=0.02, \quad (1)$$

where $\langle\alpha^2\rangle_{Av}$ is the mean square angle of the electrons emerging from the target. From the results of multiple scattering theory, it has been shown[12] that $\langle\alpha^2\rangle_{Av}\approx 0.6Z\bar{\Delta}/T_0(T_0+1)$, where $\bar{\Delta}$ is the average energy loss of the electrons that pass through the target, and T_0 is the initial electron kinetic energy in Mev. Therefore, the target thicknesses that satisfy the above requirements are approximately 54 μg/cm^2 ($\approx$2000 angstroms) for aluminum and 16 μg/cm^2 ($\approx$85 angstroms) for gold.

To prepare such thin targets, aluminum and gold were evaporated onto thin films of collodion mounted on 2-inch diameter aluminum target holders. The average thickness of each film (collodion, aluminum, and gold) was determined from weight measurements made with microbalances having sensitivities of approximately 0.2 μg and 5 μg. The results are as follows: (1) the thickness of the collodion backing for each target was approximately 5 μg/cm^2, (2) the thickness of the aluminum films were 17.3$\pm$0.8 μg/cm^2 and 38.2 $\pm$1.4 μg/cm^2, (3) the thickness of the gold films were 9.9$\pm$0.5 μg/cm^2 and 22.1$\pm$1.0 μg/cm^2. With these thin targets, electron scattering effects were negligible as demonstrated by the fact that the final cross-section values for a given target material were independent of the target thickness within experimental error.

A correction for the radiation from the collodion backing (as well as from other background) was made by subtracting the intensity measured with only a collodion target in the electron beam from the intensity measured with the collodion plus the aluminum (or gold) target. Because of the low effective Z of the collodion compared to that of the evaporated films, the relative radiation intensity from the collodion was found to be small even though its relative thickness is not negligible.

In order not to cause any excessive target heating and deterioration during the measurements, it was necessary to keep the target currents as small as possible. Because we used a high-efficiency detector and a favorable geometry with a relatively large solid angle (see Sec. A), we were able to obtain adequate counting rates with target currents less than 1 microampere. With these small target currents there was no evidence of any target deterioration, as shown by the consistency of the data for repeated sets of measurements.

Variations in the thickness of a given target for $\frac{1}{4}$-inch segments (focal-spot diameter) over the total area were expected to be small because of the large source-target distance used in the evaporation. The uniformity in the thickness of each target was checked in the following manner. The 2-inch diameter film was weighed and then the $\frac{3}{4}$-inch diameter portion concentric with the focal spot was removed with a steel punch and weighed. The average thicknesses for the two areas agreed within 10%. The final thickness that was used for each film represents the average value for the two areas, and the error limits include the systematic errors in addition to the statistical weighing errors.

The purity of the aluminum and gold wires that were evaporated was better than 99.7%, with iron and silicon as the chief impurities. At the evaporating temperature for aluminum, the vapor pressure for these impurities is negligible. It is estimated that the error introduced in the photon flux density by any impurities in the evaporated films including oxide coatings is less than 2%.

C. Photon Flux Determination

In order to evaluate the bremsstrahlung differential cross section, it is necessary to determine the photon flux $P(k,\theta)$, defined as the number of photons emitted from the target in the solid angle Ω per unit energy interval at energy k and angle θ for a given total electron charge incident on the target. The manner in which $P(k,\theta)$ is calculated from the measured pulse-height distribution $N(h)$ has been described in detail elsewhere.[11] For the data obtained in the present measurements it was found that the correction curve shown in Fig. 2 is needed to convert $N(h)$ to $P(k,\theta)$. This curve includes corrections for the following effects:

(a) The pulse-height response of the spectrometer to monoenergetic photons in the energy range below 50 kev. This response curve was measured with the 22-kev photons from Cd^{109} (see Sec. A).

(b) The spectrometer photon detection efficiency below 50 kev. This efficiency was calculated from the

[11] J. W. Motz, Phys. Rev. **100**, 1560 (1955).

[12] C. H. Blanchard, *Electron Physics*, National Bureau of Standards Circular No. 527 (U. S. Government Printing Office, Washington, D. C., 1954), p. 9.

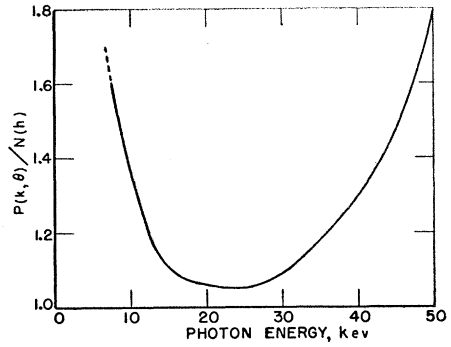

FIG. 2. Correction curve for converting a measured pulse-height spectrum $N(h)$ to a corresponding photon spectrum $P(k,\theta)$ where k is the photon energy and θ is the emission angle. The curve includes corrections for the pulse-height response of the spectrometer to monoenergetic photons, the photon detection efficiency of the spectrometer, and the photon absorption in the 20-mil beryllium window of the target chamber and in the 1-mil aluminum window over the NaI crystal (see Fig. 1).

total absorption coefficients given by Grodstein[13] and includes corrections[14] for the escape of the iodine K x-rays.

(c) The photon absorption[13] in the 20-mil beryllium window of the target chamber and in the 1-mil aluminum window covering the NaI crystal (see Fig. 1).

To correct for the background radiation, the measurements at each angle were repeated with only the collodion film in the target position. This total background was found to be less than 10% of the radiation over most of the energy spectrum from any of the aluminum or gold targets used. The fact that this background showed only about a 10% variation over the whole angular range indicates that electron scattering effects in the target chamber are small. Scattered electrons were prevented from striking the beryllium window of the target chamber with the aid of a sweep magnet (Fig. 1). No K x-rays were detected from the aluminum lining of the target chamber or from the edges of the copper slits shown in Fig. 1.

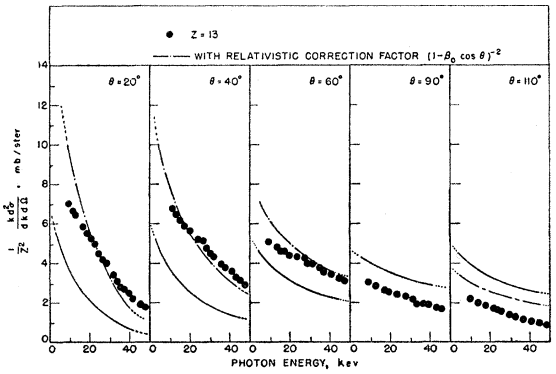

FIG. 3. 50-kev bremsstrahlung differential cross sections for aluminum at photon energies k and emission angles θ. The experimental values are shown by the closed circles which do not include the systematic-error limits. The solid curves represent the Sommerfeld cross sections calculated by Kirkpatrick and Wiedmann[2] and the dot-dashed curves are the same cross sections multiplied by the relativistic correction factor $(1-\beta_0\cos\theta)^{-2}$.

[13] Gladys White Grodstein, National Bureau of Standards Circular No. 583, 1957.

[14] T. B. Novey, Phys. Rev. 89, 672 (1953).

III. EXPERIMENTAL RESULTS AND ERRORS

The experimental values for the bremsstrahlung differential cross section $d\sigma$ are given in Figs. 3 and 4. Figure 3 shows the results with the aluminum target for photon emission angles θ of 20, 40, 60, 90, and 110 degrees, and Fig. 4 shows the results with the gold target for angles of 10, 30, 50, 90, and 110 degrees. The experimental results obtained for other angles (10, 30, 50, 70, and 140 degrees for aluminum and 20, 40, 60, 70, and 140 degrees for gold) are not included in Figs. 3 and 4 for the sake of clarity (see Figs. 8, 9, and 10). The solid and dot-dashed lines in these figures represent the theoretical estimates of the cross section: the solid lines show the Kirkpatrick-Wiedmann[2] cross sections, and the dot-dashed lines represent these cross sections multiplied by the relativistic correction factor $(1-\beta_0\cos\theta)^{-2}$. (See Sec. IV for the justification of this factor.)

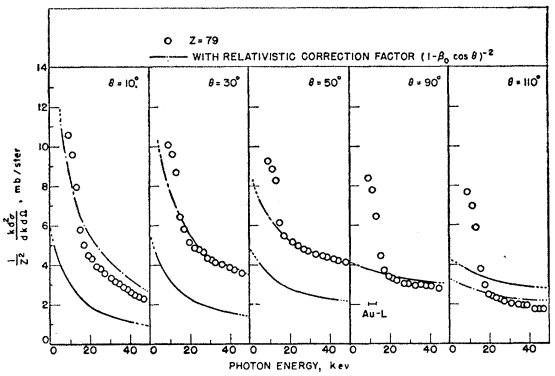

FIG. 4. 50-kev bremsstrahlung differential cross sections for gold at photon energies k and emission angles θ. The experimental values are shown by the open circles which do not include the systematic-error limits. The solid curves represent the Sommerfeld cross sections calculated by Kirkpatrick and Wiedmann[2] and the dashed curves are the same cross sections multiplied by the relativistic correction factor $(1-\beta_0\cos\theta)^{-2}$. The approximate energy range covered by the L x-rays from gold is shown on the energy scale for the 90-degree θ value.

In Fig. 4, the sharp rise in the cross section at the low photon energies is caused by the gold L radiation which covers an energy range from approximately 9.6 to 13.4 kev.[15] In order to estimate the contribution of this L radiation to the cross section, the data obtained for the 90-degree emission angle θ (Fig. 4), which appears to be fairly flat above 20 kev, was extrapolated back to 10 kev on the assumption that the spectral shape was smooth and well-behaved in the region below 20 kev; the difference between the extrapolated point and the peak measured at 10 kev was used as the

[15] S. Fine and C. F. Hendee, Nucleonics 13, No. 3, 36 (1955).

L-radiation correction at the other angles since the L radiation is expected to be emitted isotropically.

The differential cross sections shown above were integrated graphically over the photon emission angle, and the results are shown in Fig. 5. As in Figs. 3 and 4, the dot-dashed and solid curves are the theoretical cross sections with and without the relativistic correction factor. The integrated value shown for gold at 10 kev is corrected for the contribution of the gold L x-rays in the manner described above.

A final graphical integration over photon energy of the results in Fig. 5 was made to obtain the total integrated cross section ϕ_{rad}, which is defined[16] as the quantity $(1/E_0)\int_0^{E_0-\mu} k(d\sigma/dk)dk$, where E_0 is the total energy of the incident electron, μ is the electron rest energy, and k is the photon energy. The quantity $\phi_{\text{rad}}/\bar{\phi}$ is plotted in Fig. 6 as a function of the initial

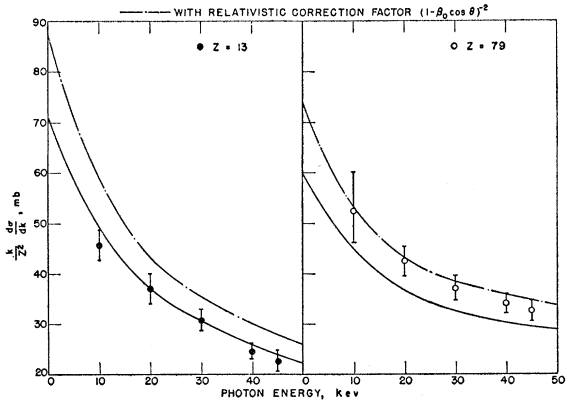

FIG. 5. 50-kev bremsstrahlung cross sections integrated over the photon emission angle θ for photon energies k. The experimental values are shown by the open and closed circles, which give the statistical- and systematic-error limits. The solid curves represent the Sommerfeld-Kirkpatrick-Wiedmann cross sections,[2] and the dot-dashed curves include the relativistic correction factor $(1-\beta_0\cos\theta)^{-2}$.

electron energy E_0, with $\bar{\phi}$ equal to $5.8\times10^{-28}Z^2$ cm^2. The energy range is extended up to higher energies in order to tie in the present measurements with previous results[11] obtained at 0.5 and 1.0 Mev. The solid curve in Fig. 6 gives the cross sections predicted by Born-approximation theory.[16] (The dashed curve indicates the screening effect for Z equal to 82.) The experimental values are given by the open (gold target) and closed (aluminum target) circles. The arrows give the approximate correction factor $Z/(Z+1)$ that would indicate the contribution of electron-electron bremsstrahlung. For an initial electron kinetic energy of 50 kev, the experimental values for $\phi_{\text{rad}}/\bar{\phi}$ are 5.5 ± 0.6 and 6.7 ± 0.7 for aluminum and gold, respectively. The theoretical value for $\phi_{\text{rad}}/\bar{\phi}$ obtained from the Kirkpatrick-Wiedmann calculations[2] for *both* aluminum and gold is

[16] W. Heitler, *The Quantum Theory of Radiation* (Oxford University Press, New York, 1954), third edition, p. 242.

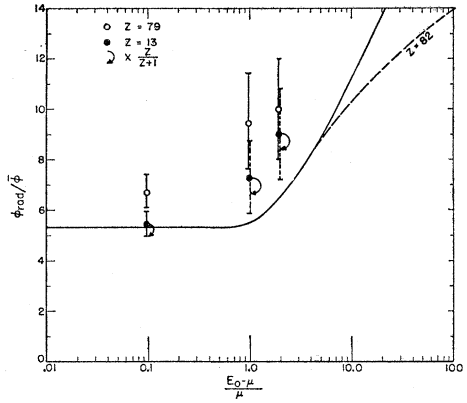

FIG. 6. Cross section for the energy lost by radiation. ϕ_{rad} is defined in reference 16, Eq. (28), E_0 and μ are the total and rest energy, respectively, of the incident electron, and $\bar{\phi}$ is $5.8\times10^{-28}Z^2$ cm^2. The experimental points for the 0.5- and 1.0-Mev electron energies were obtained from reference 11, and a rough correction for electron-electron bremsstrahlung is given by the factor $Z/(Z+1)$. The solid curve gives the cross sections obtained from relativistic Born-approximation calculations,[16] and the dashed curve indicates the screening effect for Z equal to 82. The 50-kev values of $\phi_{\text{rad}}/\bar{\phi}$ obtained from the Sommerfeld-Kirkpatrick-Wiedmann calculations[2] for both aluminum and gold are approximately 5.8, and increase to approximately 6.9 with the relativistic correction factor $(1-\beta_0\cos\theta)^{-2}$.

approximately 5.8, and with the relativistic correction factor $(1-\beta_0\cos\theta)^{-2}$, it increases to approximately 6.9.

The accuracy of the experimental values for the cross section was estimated on the basis of the following important errors:

(1) Target thickness (Sec. IIB): $\pm5\%$.

(2) Photon flux $P(k,\theta)$ (Sec. IIC): Uncertainties due to statistical errors, spectrometer corrections, window width, instability of the differential analyzer, and geometry errors are estimated to be $\pm12\%$ for the energy region above 45 kev and below 15 kev, and $\pm5\%$ over the rest of the energy spectrum.

(3) Target integrated charge (Sec. IIA): $\pm2\%$.

From a review of the above errors, the accuracy of the experimental points in Figs. 3 and 4 is estimated to be approximately 10% except for the energy region above 45 kev and below 15 kev where it is approximately 15%. In Fig. 5, the error limits of the experimental points were found from the above estimates and include the uncertainty in the L x-ray correction for gold at 10 kev. Also in Fig. 6, the error limits show an accuracy of approximately 10% for the total integrated cross section ϕ_{rad}.

IV. DISCUSSION OF RESULTS

A. Limitations of the Sommerfeld Theory

The Sommerfeld theory contains certain restrictions which must be emphasized in any comparison between theory and experiment. Specifically, we note that Sommerfeld derives a nonrelativistic matrix element in which (1) the wave functions are solutions of the

Schrödinger equation for a pure Coulomb field, and (2) retardation terms in the interaction Hamiltonian are neglected. Therefore, the Sommerfeld formula is valid only if β_0, Zr/a_0, and r/λ are small compared to unity, where a_0 is the Bohr radius of the hydrogen atom, λ is the photon wavelength, and r is the distance from the nucleus which is a parameter[17] in the bremsstrahlung cross-section formula. The question of whether the above conditions are satisfied in the present measurements will now be considered.

B. Relativistic Correction

The present measurements have been made for a value of β_0 equal to approximately 0.4, which certainly is not negligible compared to unity. Therefore the Sommerfeld-Kirkpatrick-Wiedmann cross sections[2] computed for this electron energy require a relativistic correction.

A simple estimate of the relativistic effect on the Sommerfeld cross sections[2] can be made by referring to the Born-approximation bremsstrahlung calculations.[16] A comparison of the relativistic [reference 16, Eq. (13)] and the nonrelativistic [reference 16, Eq. (17)] cross sections, $d\sigma_R$ and $d\sigma_{NR}$, respectively, gives the result that for the limiting cases where $k\rightarrow 0$ and $k\rightarrow(E_0-\mu)$,

$$d\sigma_R \approx (1-\beta_0\cos\theta)^{-2} d\sigma_{NR}. \quad (2)$$

This relativistic correction factor is derived with free-particle wave functions. Therefore the corrected cross sections must be considered only as rough estimates of the exact cross sections that would be obtained with relativistic Coulomb wave functions. Also, it should be noted that this factor does *not* correct for the retardation effects which have been neglected in the Sommerfeld-Kirkpatrick-Wiedmann calculations.[2]

C. Retardation and Screening Effects

Retardation effects are contained in the r/λ terms that arise in the expansion of the interaction Hamiltonian of the electron with the radiation field. The parameter r is difficult to evaluate accurately, and it covers a wide range of values for a given photon energy and angle. We can make an order of magnitude estimate of the importance of retardation for the conditions in our measurements by letting r equal[17] $\hbar c/q$, where q is the momentum transferred to the nucleus. For a given photon energy and angle, r was evaluated for the most probable value of q given by the Born-approximation differential cross section [reference 16, Eq. (13)]. The resulting r values, $\hat{r}$, are contained in the retardation term, $\hat{r}/\lambda$, which is plotted in Fig. 7 as a function of θ for the extreme photon energies near zero and 50 kev. (The $\hat{r}/\lambda$ values for $k\rightarrow 0$ can be expected to become negligible when screening effects are included in the theory.) We emphasize again that Fig. 7 gives only a rough estimate of the retardation terms and can easily be in error by more than a factor of two. However, the order of magnitude of these estimates indicates that retardation effects cannot be neglected for 50-kev bremsstrahlung.

A rough correction[18] for retardation effects can be made for the case where high-energy photons ($k\approx 50$ kev) are emitted from a low-Z target. The nonrelativistic matrix element *including retardation* is expressed[19] as

$$M=\int \psi_F^* e^{-i\mathbf{k}\cdot\mathbf{r}} \operatorname{grad}_A \psi_0 d\tau, \quad (3)$$

where ψ_0 and ψ_F are the initial and final wave functions and the remaining terms are defined by Schiff.[19] The nonretarded matrix element, M_s, is obtained by neglecting retardation terms, so that in the above expression $e^{-i\mathbf{k}\cdot\mathbf{r}}$ is replaced by unity. With a low-Z target the distortion produced in the wave functions by the Coulomb field is small, and for photon energies in the region of 50 kev the angular distribution of the recoil electrons is nearly isotropic. Therefore we can represent ψ_0 by a free-particle wave function $e^{i\mathbf{p}_0\cdot\mathbf{r}}$ and ψ_F by a spherically symmetric wave function $e^{i\mathbf{p}\cdot\mathbf{r}}/r$ where $\mathbf{p}_0$ and $\mathbf{p}$ are the initial and final electron momenta, respectively. With these simple types of wave functions, the matrix elements can be readily evaluated to give the retardation correction factor

$$|M|^2/|M_s|^2=[p_0^4/(p_0^2+k^2)^2](1-\beta_0\cos\theta)^{-2}, \quad (4)$$

where p_0 and k are given in units of mc and mc^2, respectively. A comparison of this result with Eq. (2) illustrates that the relativistic and retardation correction factors are approximately equal.

The K-shell Bohr radii a_0/Z for gold and aluminum are approximately 0.7×10^{-10} cm and 4.0×10^{-10} cm, respectively. These values are of the same order of

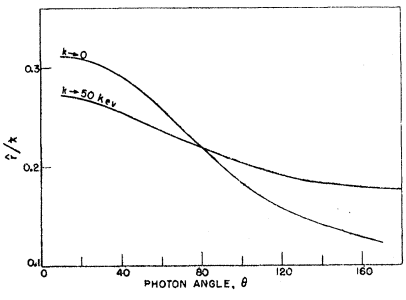

FIG. 7. Dependence of the retardation expansion parameter r/λ on photon energy k and angle θ. The most probable distance from the nucleus $\hat{r}$ which contributes to the bremsstrahlung cross section is estimated from Born-approximation calculations,[16] and λ is the wavelength of the emitted photon.

[17] The meaning of r as an impact parameter in the classical sense is discussed in reference 16, p. 248.

[18] This retardation correction factor was calculated by Mr. John Avery.

[19] L. I. Schiff, *Quantum Mechanics* (McGraw-Hill Book Company, Inc., New York, 1949), first edition, p. 243.

magnitude (10^{-10} cm) as the $\hat{r}$ values that are calculated from Fig. 7 for 50-kev photons. For lower photon energies especially below 30 kev, the $\hat{r}$ values increase up to about 10^{-8} cm. This comparison shows that screening effects may be important over the whole range of photon energies for both aluminum and gold.

D. Comparison with Theory

In the preceding Secs. B and C, we found that the nonrelativistic Sommerfeld theory is not strictly valid for the energy region covered by the present measurements, and corrections must be made for relativistic, retardation, and screening effects. In the absence of more exact calculations, rough corrections have been introduced for the relativistic and retardation effects but not for screening. These corrections are expected to be more valid for low-Z targets. In addition the retardation correction factor applies only for high-energy photons in the region of the 50-kev limit.

In Figs. 3 to 5, the experimental results are compared with the Sommerfeld-Kirkpatrick-Wiedmann cross sections[2] multiplied only by the *relativistic* correction factor (dot-dashed curve). Figures 3 and 4 indicate that the closest agreement over the whole spectrum between experiment and theory for both the aluminum and gold targets is obtained at a photon emission angle of approximately 50 degrees. As θ approaches the extreme values of zero and 180 degrees, there is an increasing departure of the experimental points from the theoretical curves. For the integrated cross sections shown in Fig. 5, the experimental values for gold show good agreement with the theory, while the values for aluminum are smaller than the theoretical (dot-dashed) curve and coincidentally show good agreement with the solid curve that does not include the relativistic correction factor.

A more detailed comparison of the results is obtained by studying the upper and lower energy regions. Figure 8 shows the angular dependence of the bremsstrahlung cross section for 45-kev photons from aluminum and gold. The theoretical curves shown by the

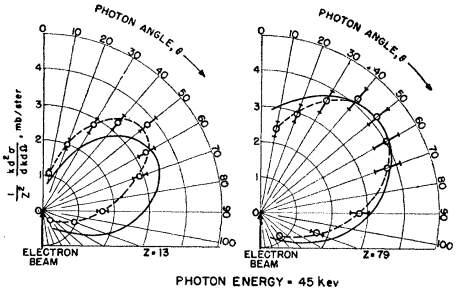

FIG. 8. Angular dependence of the bremsstrahlung cross section for 45-kev photons. The experimental values for aluminum and gold are given by the open circles and the dashed curve is an approximate fit for the experimental results over the whole angular range. The Sommerfeld-Kirkpatrick-Wiedmann cross sections[2] including the relativistic correction factor $(1-\beta_0\cos\theta)^{-2}$ are given by the solid curve.

FIG. 9. Angular dependence of the bremsstrahlung cross section for 45-kev photons emitted from an aluminum target. The experimental values are given by the open circles. The solid line is predicted by the Sommerfeld theory[2] after rough corrections have been made for relativistic, retardation, and screening effects. The dot-dashed curve is predicted by Sommerfeld[20] from classical theory, and the dashed curve is predicted from the relativistic calculations of Scherzer.[21]

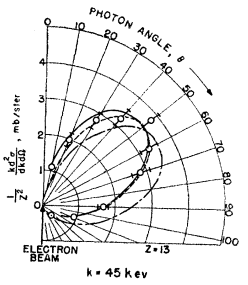

solid lines include *only* the relativistic correction factor and the dashed curves represent an approximate fit for the experimental results. For gold, the experimental points show good agreement with the theoretical curve especially at the 50-degree peak intensity angle; for angles larger and smaller than the peak angle, there is a narrowing in the experimental angular distribution curve which is suggestive of the radiation pattern from a target with a lower effective Z than gold. On the other hand, the experimental curve for aluminum is tipped more forward than the theoretical curve. The maximum difference between the experimental and theoretical results is about 25% for gold and 50% for aluminum.

The above comparison shows that for 45-kev photons, the relativistic correction factor brings the Sommerfeld-Kirkpatrick-Wiedmann cross sections[2] and the experimental results in closer agreement for the high-Z than for the low-Z target. Since this correction is not expected to be accurate for high Z, it may roughly represent the combined correction factor that would be obtained if both the retardation and relativistic effects for high Z were accurately evaluated.

To resolve the low-Z discrepancies shown in Fig. 8 for aluminum, we now will include the effect of retardation. After corrections have been made for *both* relativistic and retardation effects from the results of Secs. B and C, the angular dependence of the bremsstrahlung cross section, $d\sigma$, for 45-kev photons can be written as

$$d\sigma = A(Z_{\text{eff}}/Z_{\text{Al}})^2[p_0^4/(p_0^2+k^2)^2][1-\beta_0\cos\theta]^{-4}d\sigma_S, \quad (5)$$

where $d\sigma_S$ is the Sommerfeld-Kirkpatrick-Wiedmann cross section,[2] Z_{Al} is the atomic number for aluminum, Z_{eff} is the effective atomic number for aluminum if screening is important, and A is a normalizing factor that probably arises because the distortion of the wave functions produced by the Coulomb field from the aluminum nucleus is not negligible. From the estimates of the screening parameters given in Sec. C, we shall select 11 as a reasonable value for Z_{eff}. Then for a value of A equal to 0.9, the cross sections calculated from Eq. (5) are shown in Fig. 9 by the solid line, which shows remarkably good agreement with the experimental results. Other *relativistic* predictions of the angular distribution for photons near the high-

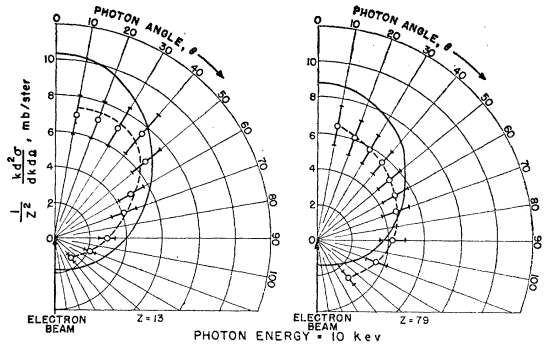

FIG. 10. Angular dependence of the bremsstrahlung cross section for 10-kev photons. The experimental values for aluminum and gold are given by the open circles and the dashed curve is an approximate fit for the experimental results over the whole angular range. The Sommerfeld-Kirkpatrick-Wiedmann cross sections including the relativistic correction factor $(1-\beta_0\cos\theta)^{-2}$ are given by the solid curve.

energy limit have been made by Sommerfeld[20] and Scherzer.[21] Sommerfeld derived the following expression from classical theory:

$$d\sigma\sim\sin^2\theta\left(1-\frac{\beta_0}{2}\cos\theta\right)^{-6}. \tag{6}$$

Scherzer's relativistic calculations which are valid for $Z\ll 137\beta_0$, give the result that

$$d\sigma\sim\sin^2\theta\left\{\frac{2(1-\beta_0^2)^{\frac{3}{2}}}{(1-\beta_0\cos\theta)^4}+\frac{[1-(1-\beta_0^2)^{\frac{1}{2}}][1-3(1-\beta_0^2)^{\frac{1}{2}}]}{2(1-\beta_0\cos\theta)^3}\right\}. \tag{7}$$

The results given by Eqs. (6) and (7) are normalized so that the peak values coincide with that given by Eq. (5), and are plotted in Fig. 9 where the dot-dashed curve gives the Sommerfeld values and the dashed curves give the Scherzer values. The Scherzer curve shows much better agreement with the experimental results than the Sommerfeld curve, although the Scherzer values appear to be too low at the small angles.

Figure 10 gives the angular distribution for 10-kev photons from the aluminum and gold targets. The theoretical curves shown by the solid lines include *only* the relativistic correction factor and the dashed curves represent an approximate fit for the experimental results. For the smaller angles, the theoretical curves overestimate the experimental cross sections. Such a difference is not surprising in view of the fact that this is the energy and angular region where screening effects become most important. In the case of the gold target, the experimental values at the larger angles are greater than the theoretical values; this discrepancy may be due to the inadequacy of the relativistic correction factor for high Z. For these low-energy photons, the experimental results show a maximum difference with the theoretical curve of approximately 30% for aluminum and 40% for gold.

In Fig. 6, the experimental values for $\phi_{\rm rad}/\bar{\phi}$ are 6.7 ± 0.7 and 5.5 ± 0.6 for gold and aluminum respectively. The difference in these values for low and high Z is consistent with the differences obtained in previous measurements[11] for higher electron energies of 500 and 1000 kev. The value for aluminum in the present measurement fortuitously shows good agreement with the Born-approximation estimate. In comparison, the $\phi_{\rm rad}/\bar{\phi}$ value obtained from the Kirkpatrick-Wiedmann calculations[2] for *both* aluminum and gold is approximately 5.8, and increases to approximately 6.9 with the relativistic correction factor $(1-\beta_0\cos\theta)^{-2}$.

ACKNOWLEDGMENTS

We wish to thank Mr. John Avery for estimating the effects of retardation and Dr. I. Oppenheim for suggestions concerning the limitations of the Sommerfeld theory. We are also grateful for the helpful discussions with Dr. H. O. Wyckoff, Dr. M. Danos, and Dr. H. W. Koch.

[20] A. Sommerfeld, Ann. Physik **11**, 257 (1931).
[21] O. Scherzer, Ann. Physik **13**, 137 (1932).